Energy Proceedings
Vol 60, 2025
ISSN 2004-2965

Decentralized Virtual Inertial and Damping Control of Multi-bus DC Microgrid#

Xuecheng Li[1], Changbin Hu[2,3*], Shanna Luo[2], Gaowei Wang[2], Xuebin Li[2], Dawei Qi[2]

1 University of Duisburg-Essen, 47057, Duisburg, Germany

2 North China University of Technology, 100144, Beijing, China
3 Haihe Laboratory of Information Technology Application Innovation, 300270, Tianjin, China
(changbinlove@ncut.edu.cn)

ABSTRACT

Virtual Inertia Damping Control (VID-Control) is an effective method to improve the inertia and damping of DC microgrids. However, unreasonable design of additional inertia (J) and damping (D)parameters will lead to severe system oscillations or even instability. To address this issue, this paper proposes a VID-Control strategy for multi-bus DC microgrids based on an extended observer. Leveraging Lyapunov stability theory, this strategy enables the decentralized design of virtual inertia, damping and the low-level fast voltage control. It does not require measurements of the converter's own output current or parameters of other converters. This not only realizes decentralized control design of VID-Control in multi-bus DC microgrids but also reduces the cost of output current sensors while enhancing the system's inertia and damping. The effectiveness of the proposed method is verified through simulations of multi-DC buck converter system.

Keywords: DC Microgrid, Virtual Inertia and Damping Control, Lyapunov stability, DC-DC converter, buck converter, Disturbance Observer.

1. INTRODUCTION

DC microgrids offer advantages such as fewer conversion levels, high efficiency, and easy integration of distributed renewable energy, energy storage, and charging systems, thus exhibiting broad development prospects[1], and are gradually evolving from small-scale single-bus systems to large-scale multi-bus systems[2]. However, most distributed generators (DGs) in DC microgrids are connected to the grid via power electronic converter interfaces, which have small inertia, and the output voltage is significantly affected by load variations[3]. Stability issues caused by interactions between converters have become increasingly prominent, which is a key challenge to the widespread application of multi-bus DC microgrids.

To enhance the inertia and voltage stability of DC microgrids, current control strategies mainly include inertial droop control, virtual DC machine control, and virtual inertia damping control (VID-Control)[4]. VID-Control retains the linear characteristics of the system and the droop coefficients of each converter while flexibly simulating the equivalent inertia and damping characteristics of converters. It not only improves system inertia but also adjusts the system's damping to avoid potential oscillation problems caused by large inertia[5]. Owing to its better adaptability and design flexibility, VID-Control has been extensively studied recently. For instance, an adaptive VID-Control strategy was designed to improve system inertia and damping while maintaining favorable transient performance[6].

In DC microgrids with multiple converters, mismatches between droop coefficients, virtual inertia, and damping parameters can easily result in energy oscillations between converters, putting the system at risk of instability[4]. To address the coordinated operation of multiple converters, common design methods either ensure that the transient responses of bus voltage and current at the output of each converter are as synchronized as possible to reduce energy oscillations between converters[7], or equivalize multiple parallel converters to a single converter with larger capacity and then design parameters such as virtual damping, inertia, and droop coefficients for this single equivalent converter[8]. Another commonly used impedance-based control parameter design method requires detailed impedance parameters of the whole system[9]. For multi-bus DC microgrids, obtaining detailed global system parameters is difficult; moreover, if the system composition varies or restructured, the control parameters need to be redesigned, resulting in low flexibility.

Nevertheless, all the afore-mentioned studies focus on VID-Control for single-bus DC Microgrid. For multi-bus

This work was supported by the National Key R&D Program of China through Renewable Energy Technology Special Projects (project No. 2024YFB4207300), and Tianjin Natural Science Foundation (project No. 24JCYBJC01090)
This is a paper for the 5th Applied Energy Symposium and Forum: Renewable Energy Matrix (REM2025), Oct. 29-31, 2025, Yancheng, China.

DC microgrid, these methods are hardly applicable due to the existence of line impedance between buses and changes in load positions. With the increasing penetration of distributed energy sources and the expansion of microgrid scale, research on control strategies for multi-bus DC microgrids has become essential.

Note that the low-level fast voltage control of converters originally does not require output current measurement. Therefore, output current observer-based VID-Control can be integrated into the converter's voltage control without modifying the converter hardware (without adding output current sensors), thereby reducing hardware costs[10]. However, compared with current sensors, disturbance observers have inherent dynamic characteristics, leading to a certain (phase) delay in the observed output current relative to the directly measured output current. To best of authors knowledge, there have been no reports on observer-based VID-Control for single- or multi-bus DC microgrids.

To solve the above problems, this paper proposes a decentralized observer-based VID-Control strategy for multi-bus DC microgrids. The advantages of this strategy are as follows:

1. The output current observer eliminates the need for hardware modifications and reduces hardware costs;
2. Under a given droop coefficient, virtual inertia and damping parameters can be decentralized designed to enhance system inertia and voltage stability.

2. PRIMARY VOLTAGE CONTROL MODELLING OF MULTI-BUS DC MICROGRID

2.1 Overall System Control Structure

The research object of this paper is a multi-bus DC microgrid as shown in Fig. 1, where buses are connected via lines. Each bus is connected to an equivalent aggregated DG. Each DG adopts low-level primary fast voltage tracking control (inner voltage control loop), and higher-level virtual inertia damping control (outer inertia loop). Under a specific droop coefficient, the outer inertia loop can freely adjust the inertia and damping of the DG to improve the system's characteristics. In addition, an output current observer is used instead of actual output current measurement, enabling the integration of virtual inertia damping control into the DG's low-level fast voltage control without adding extra output current sensors.

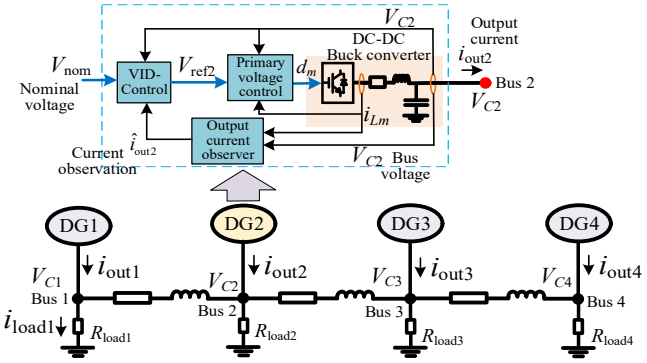

Fig. 1 Observer-based VID-Control of multi-bus DC Microgrid

2.2 Modeling of a Single Buck Converter

The physical layer of a multi-bus DC microgrid includes DGs, physical lines, and loads. First, each DG is includes a buck converter consisting of PWM module and an LC filter. Due to high PWM switching frequency, the buck converter can be simplified to an averaged LC filter model, whose state-space model of DGm is as follows:

$$\begin{aligned} \dot{\boldsymbol{x}}_m &= \boldsymbol{A}_m^{\mathrm{sg}} \boldsymbol{x}_m + \boldsymbol{B}_m u_{\mathrm{km}} + \boldsymbol{E}_m i_{\mathrm{outm}} \\ \boldsymbol{y}_m &= \boldsymbol{x}_m \end{aligned} \tag{1}$$

where $\boldsymbol{y}_m = \boldsymbol{x}_m = \begin{bmatrix} V_{Cm} \\ i_{Lm} \end{bmatrix}$, $\boldsymbol{A}_m^{\mathrm{sg}} = \begin{bmatrix} 0 & \frac{1}{C_m} \\ -\frac{1}{L_m} & -\frac{R_{Lm}}{L_m} \end{bmatrix}$, $\boldsymbol{B}_m = \begin{bmatrix} 0 \\ \frac{1}{L_m} \end{bmatrix}$, $\boldsymbol{E}_m = \begin{bmatrix} -\frac{1}{C_m} \\ 0 \end{bmatrix}$, the state variable $\boldsymbol{x}_m$ and output $\boldsymbol{y}_m$ are both the capacitor voltage (bus voltage) V_{Cm} and inductor current i_{Lm}; the control signal u_{km} is the PWM duty; i_{outm} is the output current of the converter; C_m, L_m, and R_{Lm} are the filter capacitor, filter inductor, and internal resistance of the filter inductor, respectively.

2.3 Modeling of Inter-connected Converters in Multi-bus DC Microgrid

Low-voltage converters are interconnected via resistive lines to form a multi-bus DC microgrid. The state-space model of the physical interconnected multi-converter is as follows:

$$\begin{aligned} \dot{\boldsymbol{x}}_m &= \boldsymbol{A}_{mm} \boldsymbol{x}_m + \sum_{n \in N_m} \boldsymbol{A}_{mn} \boldsymbol{x}_n + \boldsymbol{B}_m u_{\mathrm{km}} + \boldsymbol{E}_m i_{\mathrm{loadm}} \\ \boldsymbol{y}_m &= \boldsymbol{x}_m \end{aligned} \tag{2}$$

where state variables $\boldsymbol{x}_n = \begin{bmatrix} V_{Cn} \\ i_{Ln} \end{bmatrix}$ are capacitor (bus) voltage and inductor current of the adjacent converter n;

$\boldsymbol{A}_{mn}=\begin{bmatrix}\frac{1}{C_m R_{mn}} & 0\\ 0 & 0\end{bmatrix}$, $\boldsymbol{A}_{mm}=\begin{bmatrix}\sum_{n\in N_m}\frac{-1}{C_m R_{mn}} & \frac{1}{C_m}\\ -\frac{1}{L_m} & \frac{-R_{Lm}}{L_m}\end{bmatrix}$, $i_{\mathrm{load}m}$ is the load current; R_{mn} is the connecting line resistance between converter m and n.

2.4 Low-level Fast Voltage Control of Buck Converter

The low-level fast voltage control of converters includes dual PI loop control and state feedback control. State feedback control directly feeds back the capacitor voltage, inductor current, and voltage error integral e_V. Compared with dual PI loop control, state feedback control has a shorter control link, a simpler control structure, and can precisely regulate system poles and dynamic performance, facilitating easier analysis and optimization of system stability. The state-feedback fast voltage control is given as:

$$\begin{aligned}\dot{e}_{Vm}&=V_{\mathrm{ref}m}-V_{Cm}\\ u_{\mathrm{k}m}&=k_{3m}e_{Vm}+[k_{1m},\,k_{2m}]\boldsymbol{y}_m\end{aligned}\tag{3}$$

where e_{Vm} is the capacitor voltage error integral state variable; k_{1m}, k_{2m} and k_{3m} are the control gain coefficients for the capacitor voltage V_{Cm}, inductor current i_{Lm}, and voltage error integral e_{Vm}, respectively. Substituting the voltage control Eq. (3) into Eq. (1), the state-space model of the low-level closed-loop voltage control of converter m is obtained:

$$\begin{aligned}\dot{\boldsymbol{x}}_m^V&=\boldsymbol{A}_m^V\boldsymbol{x}_m^V+\boldsymbol{B}_m^V V_{\mathrm{ref}m}+\boldsymbol{E}_m^V i_{\mathrm{out}m}\\ \boldsymbol{y}_m^V&=\boldsymbol{x}_m^V\end{aligned}\tag{4}$$

where $\boldsymbol{x}_m^V=\boldsymbol{y}_m^V=\begin{bmatrix}V_{Cm}\\ i_{Lm}\\ e_{Vm}\end{bmatrix}$, $\boldsymbol{A}_m^V=\begin{bmatrix}0 & 1/C_m & \\ \frac{k_{1m}-1}{L_m} & \frac{k_{2m}-R_{Lm}}{L_m} & \frac{k_{3m}}{L_m}\\ & & -1\end{bmatrix}$,

$\boldsymbol{B}_m^V=\begin{bmatrix}0\\ 0\\ 1\end{bmatrix}$, $\boldsymbol{E}_m^V=\begin{bmatrix}-1/C_m\\ 0\\ 0\end{bmatrix}$.

3. OBSERVER-BASED VID-CONTROL DESIGN

3.1 Output Current Observer Model of Converter

The low-level voltage control of converters usually only relies on the measurements of inductor current and capacitor voltage. However, the output current of the converter is required for designing virtual inertia damping control or droop parallel control. In this paper, an output current observer is designed to realize output current estimation and virtual inertia damping control without introducing sensor hardware. This enables the system equipment to have a certain capability of automatic load power sharing and enhances the system's inertia and damping. Based on the converter's state-space model in Eq. (1), the converter's output current (disturbance) observer is designed as follows:

$$\begin{aligned}\dot{\hat{\boldsymbol{x}}}_m&=\boldsymbol{A}_m^{\mathrm{sg}}\hat{\boldsymbol{x}}_m+\boldsymbol{L}_{\mathrm{obs},m}(\boldsymbol{y}_m-\hat{\boldsymbol{y}}_m)+\boldsymbol{E}_m\hat{i}_{\mathrm{out}m}+\boldsymbol{B}_m u_{\mathrm{k}m}\\ \dot{\hat{i}}_{\mathrm{out}m}&=\boldsymbol{L}_{im}^{\mathrm{obs}}(\boldsymbol{y}_m-\hat{\boldsymbol{y}}_m)=\boldsymbol{L}_{im}^{\mathrm{obs}}\boldsymbol{x}_m-\boldsymbol{L}_{im}^{\mathrm{obs}}\hat{\boldsymbol{x}}_m\\ \hat{\boldsymbol{y}}_m&=\hat{\boldsymbol{x}}_m,\quad \hat{i}_{\mathrm{out}m}=\hat{i}_{\mathrm{out}m}\end{aligned}\tag{5}$$

where $\hat{\boldsymbol{x}}_m$ is the estimated value of the state variables $\boldsymbol{x}_m$ (capacitor voltage and inductor current); $\boldsymbol{L}^{\mathrm{obs}}{}_{xm}$ is the Luenberger state observer gain matrix of the converter; $\hat{i}_{\mathrm{out}m}$ is the observed value of the output current; $\boldsymbol{L}^{\mathrm{obs}}{}_{im}$ is the horizontal vector of the output current (disturbance) observation gain. In this paper, the voltage and current observation poles of the converter state observer are set to 5 times the original voltage and current poles of the converter in Eq. (1); the output current observation pole is set to -300 to achieve fast observation of the output current while avoiding excessive sensitivity of the observation to ripples.

3.2 Observer-based VID-Control of Converters

Based on the observed output current, the VID-Control is designed as:

$$\begin{aligned}\Delta\dot{V}_{\mathrm{ref},m}&=-\frac{D_m}{J_m}\Delta V_{\mathrm{ref},m}+\frac{1/k_{\mathrm{d},m}-D_m}{J_m}(V_{\mathrm{nom}}-V_{Cm})-\frac{1}{J_m}\hat{i}_{\mathrm{out}m}\\ V_{\mathrm{ref},m}&=V_{\mathrm{nom}}+\Delta V_{\mathrm{ref},m}\end{aligned}\tag{6}$$

where $\Delta V_{\mathrm{ref},m}$ is the inertia state variable and the reference adjustment for the low-level voltage control; $V_{\mathrm{ref},m}$ is the voltage reference value for the low-level voltage control; V_{nom} is the rated voltage of DC Microgrid; virtual inertia J_m, virtual damping D_m, and droop coefficient $k_{\mathrm{d},m}$ of VID-Control are all greater than 0.

3.3 Closed-Loop Control Model of Multi-bus DC Microgrid

To obtain the closed-loop model of whole multi-bus DC microgrid with low-level voltage control and higher-level VID-control, substitute the observed output current value in Eq. (5) into Eq. (6), then substitute the VID-Control output $V_{\mathrm{ref},m}$ into the low-level voltage control in Eq. (3), finally substitute the voltage control signal $u_{\mathrm{k}m}$ into the state-space model of the interconnected physical system in Eq. (2). The closed-loop state-space model of the overall DC Microgrid is obtained:

$$\begin{aligned}\dot{\boldsymbol{x}}_m^{\mathrm{gl}}&=\boldsymbol{A}_{mm}^{\mathrm{gl}}\boldsymbol{x}_m^{\mathrm{gl}}+\boldsymbol{A}_{mn}^{\mathrm{gl}}\boldsymbol{x}_n^{\mathrm{gl}}+\boldsymbol{E}_{Vm}^{\mathrm{gl}}V_{\mathrm{nom}}+\boldsymbol{E}_{im}^{\mathrm{gl}}i_{\mathrm{load}m}\\ \boldsymbol{y}_m^{\mathrm{gl}}&=\boldsymbol{C}_m^{\mathrm{gl}}\boldsymbol{x}_m^{\mathrm{gl}}+\boldsymbol{D}_m^{\mathrm{gl}}V_{\mathrm{nom}}\end{aligned}\tag{9}$$

where the closed-loop control state variables and state matrix of converter m are:

$$\boldsymbol{x}_m^{\mathrm{gl}}=\begin{bmatrix}\boldsymbol{x}_m\\ e_{Vm}\\ \hat{\boldsymbol{x}}_m\\ \hat{i}_{\mathrm{out}m}\\ \Delta V_{\mathrm{ref},m}\end{bmatrix},\boldsymbol{x}_n^{\mathrm{gl}}=\begin{bmatrix}\boldsymbol{x}_n\\ \boldsymbol{x}_{\mathrm{k}n}\\ \hat{\boldsymbol{x}}_n\\ \hat{i}_{\mathrm{out}n}\\ \Delta V_{\mathrm{ref},n}\end{bmatrix},\boldsymbol{y}_m^{\mathrm{gl}}=\begin{bmatrix}\boldsymbol{y}_m\\ u_{\mathrm{k}m}\\ \hat{i}_{\mathrm{out}m}\\ \Delta V_{\mathrm{ref},m}\end{bmatrix},\boldsymbol{D}_m^{\mathrm{gl}}=\begin{bmatrix}\boldsymbol{0}_{2\times1}\\ 0\\ 0\\ 1\end{bmatrix},$$

$$\boldsymbol{A}_{mm}^{\mathrm{gl}}=\begin{bmatrix}\boldsymbol{A}_{mm}+\boldsymbol{B}_m[k_{1m},k_{2m}] & \boldsymbol{B}_m k_{3m} & \boldsymbol{0}_{2\times2} & \boldsymbol{0}_{2\times1} & \boldsymbol{0}_{2\times1}\\ \boldsymbol{B}_{\mathrm{k}m} & 0 & \boldsymbol{0}_{1\times2} & 0 & 1\\ \boldsymbol{L}_{xm}^{\mathrm{obs}}+\boldsymbol{B}_m[k_{1m},k_{2m}] & \boldsymbol{B}_m k_{3m} & \boldsymbol{A}_m^{\mathrm{sg}}-\boldsymbol{L}_{xm}^{\mathrm{obs}} & \boldsymbol{E}_m & \boldsymbol{0}_{2\times1}\\ \boldsymbol{L}_{im}^{\mathrm{obs}} & 0 & -\boldsymbol{L}_{im}^{\mathrm{obs}} & 0 & 0\\ [\frac{e_{\mathrm{vir}m}}{k_{\mathrm{d},m}}-a_{\mathrm{vir}m},0] & 0 & \boldsymbol{0}_{1\times2} & e_{\mathrm{vir}m} & a_{\mathrm{vir}m}\end{bmatrix},$$

$$\boldsymbol{A}_{mn}^{\mathrm{gl}}=\begin{bmatrix}\boldsymbol{A}_{mn} & \\ & \boldsymbol{0}_{5\times5}\end{bmatrix},a_{\mathrm{vir},m}=-\frac{D_m}{J_m},e_{\mathrm{vir},m}=-\frac{1}{J_m},$$

$$\boldsymbol{C}_m^{\mathrm{gl}}=\begin{bmatrix}I_{2\times2} & \boldsymbol{0}_{2\times1} & \boldsymbol{0}_{2\times2} & 0 & 0\\ [k_{1m},k_{2m}] & k_{3m} & \boldsymbol{0}_{1\times2} & 0 & 0\\ \boldsymbol{0}_{1\times2} & 0 & \boldsymbol{0}_{1\times2} & 1 & 0\\ \boldsymbol{0}_{1\times2} & 0 & \boldsymbol{0}_{1\times2} & 0 & 1\end{bmatrix},\boldsymbol{E}_{Vm}^{\mathrm{gl}}=\begin{bmatrix}\boldsymbol{0}_{2\times1}\\ 1\\ \boldsymbol{0}_{2\times1}\\ 0\\ a_{\mathrm{vir},m}-\frac{e_{\mathrm{vir},m}}{k_{\mathrm{d},m}}\end{bmatrix},\boldsymbol{E}_{im}^{\mathrm{gl}}=\begin{bmatrix}\boldsymbol{E}_m\\ 0\\ \boldsymbol{0}_{2\times1}\\ 0\\ 0\end{bmatrix}$$

The global state-space model of Eq. (9) is:

$$\begin{aligned}\dot{\boldsymbol{x}}^{\mathrm{gl}}&=\boldsymbol{A}^{\mathrm{gl}}\boldsymbol{x}^{\mathrm{gl}}+\boldsymbol{E}_V^{\mathrm{gl}}V_{\mathrm{nom}}+\boldsymbol{E}_i^{\mathrm{gl}}\boldsymbol{i}_{\mathrm{load}}^{\mathrm{gl}}\\ \boldsymbol{y}^{\mathrm{gl}}&=\boldsymbol{C}^{\mathrm{gl}}\boldsymbol{x}^{\mathrm{gl}}+\boldsymbol{D}^{\mathrm{gl}}V_{\mathrm{nom}}\end{aligned}\tag{10}$$

where $\boldsymbol{x}^{\mathrm{gl}}=[\boldsymbol{x}^{\mathrm{gl}}{}_1,...,\boldsymbol{x}^{\mathrm{gl}}{}_N]^{\mathrm{T}}$, $\boldsymbol{i}^{\mathrm{gl}}{}_{\mathrm{load}}=[i_{\mathrm{load}1},...,i_{\mathrm{load}N}]^{\mathrm{T}}$, $\boldsymbol{E}^{\mathrm{gl}}{}_V=[\boldsymbol{E}^{\mathrm{gl}}{}_{V1},\ ...,\ \boldsymbol{E}^{\mathrm{gl}}{}_{VN}]^{\mathrm{T}}$, $\boldsymbol{C}^{\mathrm{gl}}=\mathrm{diag}(\boldsymbol{C}^{\mathrm{gl}}{}_1,\ ...,\ \boldsymbol{C}^{\mathrm{gl}}{}_N)$, $\boldsymbol{D}^{\mathrm{gl}}{}_V=\mathrm{diag}(\boldsymbol{D}^{\mathrm{gl}}{}_{V1},\ ...,\ \boldsymbol{D}^{\mathrm{gl}}{}_{VN})$, $\boldsymbol{A}^{\mathrm{gl}}=\begin{bmatrix}\boldsymbol{A}_{11}^{\mathrm{gl}} & \cdots & \boldsymbol{A}_{1N}^{\mathrm{gl}}\\ \vdots & \ddots & \vdots\\ \boldsymbol{A}_{N1}^{\mathrm{gl}} & \cdots & \boldsymbol{A}_{NN}^{\mathrm{gl}}\end{bmatrix}$.

4. LYAPUNOV STABILITY-BASED DECENTRALIZED VID-CONTROL PARAMETER OPTIMIZATION

4.1 Lyapunov Theory-based Global Stability Analysis

Lyapunov theory is used for stability analysis and controller design:

$$V=(\boldsymbol{x}^{\mathrm{gl}})^{\mathrm{T}}\boldsymbol{P}^{\mathrm{gl}}\boldsymbol{x}^{\mathrm{gl}}\tag{11}$$

Since the system input V_{nom} and disturbance $\boldsymbol{i}^{\mathrm{gl}}{}_{\mathrm{load}}$ in Eq. (10) are considered to have no impact on the system stability, they can be ignored in the stability analysis. The time derivative of Eq. (11) is then:

$$\begin{aligned}\dot{V}&=(\dot{\boldsymbol{x}}^{\mathrm{gl}})^{\mathrm{T}}\boldsymbol{P}^{\mathrm{gl}}\boldsymbol{x}^{\mathrm{gl}}+(\boldsymbol{x}^{\mathrm{gl}})^{\mathrm{T}}\boldsymbol{P}^{\mathrm{gl}}\dot{\boldsymbol{x}}^{\mathrm{gl}}\\ &=(\boldsymbol{A}^{\mathrm{gl}}\boldsymbol{x}^{\mathrm{gl}})^{T}\boldsymbol{P}^{\mathrm{gl}}\boldsymbol{x}^{\mathrm{gl}}+(\boldsymbol{x}^{\mathrm{gl}})^{\mathrm{T}}\boldsymbol{P}^{\mathrm{gl}}\boldsymbol{A}^{\mathrm{gl}}\boldsymbol{x}^{\mathrm{gl}}\\ &=(\boldsymbol{x}^{\mathrm{gl}})^{\mathrm{T}}[(\boldsymbol{A}^{\mathrm{gl}})^{\mathrm{T}}\boldsymbol{P}^{\mathrm{gl}}+\boldsymbol{P}^{\mathrm{gl}}\boldsymbol{A}^{\mathrm{gl}}]\boldsymbol{x}^{\mathrm{gl}}<0\end{aligned}\tag{12}$$

The above Eq. (12) is equivalent to:

$$(\boldsymbol{A}^{\mathrm{gl}})^{\mathrm{T}}\boldsymbol{P}^{\mathrm{gl}}+\boldsymbol{P}^{\mathrm{gl}}\boldsymbol{A}^{\mathrm{gl}}<0\tag{13}$$

To decouple each converter from each other in the stability analysis and control design, global Lyapunov matrix $\boldsymbol{P}^{\mathrm{gl}}$ is designed as a diagonal matrix: $\boldsymbol{P}^{\mathrm{gl}}=\mathrm{diag}(\boldsymbol{P}_1, \boldsymbol{P}_2, ..., \boldsymbol{P}_m ,..., \boldsymbol{P}_N)$. The symmetric positive definite matrix $\boldsymbol{P}_m$ has the form $\boldsymbol{P}_m=\begin{bmatrix}p_{11}^m & \boldsymbol{0}_{1\times6}\\ \boldsymbol{0}_{6\times1} & \boldsymbol{P}_{6\times6}^m\end{bmatrix}$, where $p^m{}_{11}>0$ and $\boldsymbol{P}^m{}_{6\times6}$ is a 6×6 positive definite symmetric matrix. Therefore, $\boldsymbol{P}_m$ of each converter can be designed to fulfill Eq. (13). $(\boldsymbol{A}^{\mathrm{gl}})^{\mathrm{T}}\boldsymbol{P}^{\mathrm{gl}}+\boldsymbol{P}^{\mathrm{gl}}\boldsymbol{A}^{\mathrm{gl}}$ can be decomposed into a diagonal matrix (local term) and a non-diagonal matrix (coupling term):

$$\begin{aligned}&(\boldsymbol{A}^{\mathrm{gl}})^{\mathrm{T}}\boldsymbol{P}^{\mathrm{gl}}+\boldsymbol{P}^{\mathrm{gl}}\boldsymbol{A}^{\mathrm{gl}}\\ &=\begin{bmatrix}\boldsymbol{A}_{mm}^{\mathrm{gl}} & \boldsymbol{A}_{mn}^{\mathrm{gl}}\\ \boldsymbol{A}_{nm}^{\mathrm{gl}} & \boldsymbol{A}_{nn}^{\mathrm{gl}}\end{bmatrix}^{\mathrm{T}}\begin{bmatrix}\boldsymbol{P}_m & \\ & \boldsymbol{P}_n\end{bmatrix}+\begin{bmatrix}\boldsymbol{P}_m & \\ & \boldsymbol{P}_n\end{bmatrix}\begin{bmatrix}\boldsymbol{A}_{mm}^{\mathrm{gl}} & \boldsymbol{A}_{mn}^{\mathrm{gl}}\\ \boldsymbol{A}_{nm}^{\mathrm{gl}} & \boldsymbol{A}_{nn}^{\mathrm{gl}}\end{bmatrix}\\ &=\underbrace{\begin{bmatrix}(\boldsymbol{A}_{mm}^{\mathrm{gl}})^{\mathrm{T}}\boldsymbol{P}_m+\boldsymbol{P}_m\boldsymbol{A}_{mm}^{\mathrm{gl}} & \\ & (\boldsymbol{A}_{nn}^{\mathrm{gl}})^{\mathrm{T}}\boldsymbol{P}_n+\boldsymbol{P}_n\boldsymbol{A}_{nn}^{\mathrm{gl}}\end{bmatrix}}_{\text{diagonal term (local term)}}\\ &\quad+\underbrace{\begin{bmatrix} & (\boldsymbol{A}_{nm}^{\mathrm{gl}})^{\mathrm{T}}\boldsymbol{P}_n+\boldsymbol{P}_m\boldsymbol{A}_{mn}^{\mathrm{gl}}\\ \left((\boldsymbol{A}_{nm}^{\mathrm{gl}})^{\mathrm{T}}\boldsymbol{P}_n+\boldsymbol{P}_m\boldsymbol{A}_{mn}^{\mathrm{gl}}\right)^{\mathrm{T}} & \end{bmatrix}}_{\text{non-diagonal term (coupling term)}}\end{aligned}\tag{14}$$

where the coupling term between converter m and n:

$$(\boldsymbol{A}_{nm}^{\mathrm{gl}})^{\mathrm{T}}\boldsymbol{P}_n+\boldsymbol{P}_m\boldsymbol{A}_{mn}^{\mathrm{gl}}=\begin{bmatrix}\frac{p_{11}^n+p_{11}^m}{C_n}\sum_{m\in N_n}\frac{-1}{R_{mn}} & \boldsymbol{0}_{1\times6}\\ \boldsymbol{0}_{6\times1} & \boldsymbol{0}_{6\times6}\end{bmatrix}\tag{15}$$

Therefore, by minimize $p^n{}_{11}$ and $p^m{}_{11}$ of $\boldsymbol{P}_m$ and $\boldsymbol{P}_n$ such that the coupling terms $\begin{bmatrix} & (\boldsymbol{A}_{nm}^{\mathrm{gl}})^{\mathrm{T}}\boldsymbol{P}_n+\boldsymbol{P}_m\boldsymbol{A}_{mn}^{\mathrm{gl}}\\ \left((\boldsymbol{A}_{nm}^{\mathrm{gl}})^{\mathrm{T}}\boldsymbol{P}_n+\boldsymbol{P}_m\boldsymbol{A}_{mn}^{\mathrm{gl}}\right)^{\mathrm{T}} & \end{bmatrix}$ in Eq. (15) and (14) are approximately zero, the entire Eq. (14) can be made negative definite as long as the diagonal terms $\begin{bmatrix}(\boldsymbol{A}_{mm}^{\mathrm{gl}})^{\mathrm{T}}\boldsymbol{P}_m+\boldsymbol{P}_m\boldsymbol{A}_{mm}^{\mathrm{gl}} & \\ & (\boldsymbol{A}_{nn}^{\mathrm{gl}})^{\mathrm{T}}\boldsymbol{P}_n+\boldsymbol{P}_n\boldsymbol{A}_{nn}^{\mathrm{gl}}\end{bmatrix}$ in Eq. (14) are negative definite. Thus, different $\boldsymbol{P}_m$ can be designed for each converter controller to satisfy:

$$(\boldsymbol{A}^{\mathrm{gl}}{}_{mm})^{\mathrm{T}}\boldsymbol{P}_m+\boldsymbol{P}_m\boldsymbol{A}^{\mathrm{gl}}{}_{mm}<0\tag{16}$$

And minimizing $p^m{}_{11}$ and $p^m{}_{11}$ can reduce the coupling between the Lyapunov stability matrices in Eq. (14).

4.2 Bilinear Optimization-based Control Parameter Design

Finally, the objective function for optimizing the controller parameters of converter m is:

$$\min p^{m}_{11} \tag{17}$$

sub. $\boldsymbol{P}_m > 0$ and Eq. (16).

Since $\boldsymbol{A}^{sg}_{cl,m}$ and $\boldsymbol{P}_m^{dist}$ in Eq. (16) both include optimizing variables, Eq. (17) can generally not be solved via LMI optimization. Therefore, Eq. (17) is solved with Bilinear optimization, which is implemented using the MATLAB + YALMIP + Penlab bilinear optimization solver. The decentralized optimization variables for converter m include 5 variables (k_{1m},k_{2m},k_{3m}, $e_{vir,m}$, $a_{vir,m}$) and 22 variables (p_{11} and the symmetric matrix $\boldsymbol{P}^{*}_{6\times6}$), totaling 27 variables. The optimal variables obtained from the solution are k^{*}_{1m}, k^{*}_{2m}, k^{*}_{3m}, $e^{*}_{vir,m}$, $a^{*}_{vir,m}$, p^{*}_{11}, $\boldsymbol{P}^{*}_{6\times6}$. Then, the optimal virtual inertia and virtual damping are $J^{*}_{m} = -1/e^{*}_{vir,m}$ and $D^{*}_{m}=-a^{*}_{vir,m}*J^{*}_{m}$.

5. EXPERIMENTAL VERIFICATION

5.1 Experimental Test of Proposed VID-Control

To verify the effectiveness of the proposed method, the proposed observer-based VID-Control with the microgrid structure in Fig. 1 is tested in MATLAB/Simulink. The system and control parameters are given in Tab. 1.

Tab. 1 System and control parameters

parameters	values
Rated output currents $i_{rate\ 1/2/3/4}$ /A	3, 4, 3, 4
Inductance $L_{1/2/3/4}$ /mH	0.365, 0.5, 0.365, 0.5
Parastic resistance $R_{L1/2/3/4}$ /Ω	0.05, 0.06, 0.05, 0.06
Capacity $C_{1/2/3/4}$ /mF	0.3, 0.45, 0.3, 0.45
Resistance $R_{line12/23/34}$ /Ω	0.075, 0.05, 0.075
Droop coefficients $k_{d,1/2/3/4}$	0.4,0.3,0.4,0.3
Low-level voltage control gains $[k_{1m},k_{2m},k_{3m}]$ of converter 1,2,3,4	[-10,-5, 3416], [-22, -7, 7020], [-10, -5, 3416], [-22, -7, 7020]
Virtual inertia $J_{1/2/3/4}$	0.13,0.08,0.077,0.097,
Virtual damping $D_{1/2/3/4}$	9.35, 17.5, 15.9, 9.89

This experiment tests the proposed VID-Control under bus load switching. At the test start, load resistors of 12Ω, 10Ω, 12Ω, and 10Ω are connected to buses 1, 2, 3, and 4, respectively. In t=1s, an additional load $R_{load1,2,3,4}$ = 12Ω, 10Ω, 12Ω, and 10Ω are periodically connected to and disconnected from at bus 1, 2, 3, and 4, respectively, in every period connected for 1s and then disconnected for another 1s. The voltages of the 4 buses are shown in Fig. 4 and 5. It can be seen from the figures that the proposed virtual inertia damping control for multi-bus DC microgrids can stabilize the system voltage effectively. Before the additional loads are connected, the voltage is around 20.3V; after connecting the additional load, due to the voltage droop characteristic of virtual inertia damping, the voltages of the 4 buses drop to about 19.7V, with a ripple peak-to-peak value of less than 0.1V. After the additional loads are disconnected, the system voltage restored to 20.3V again.

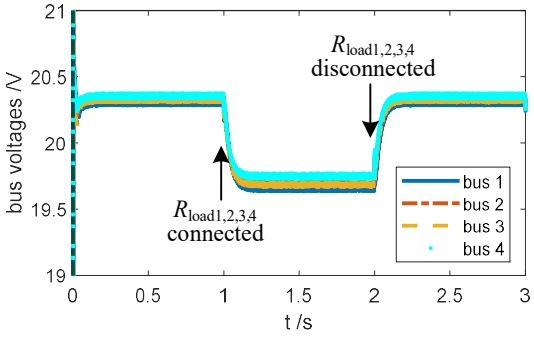

Fig. 4 Bus Voltages of the DC Microgrid with Virtual Inertia Damping Control

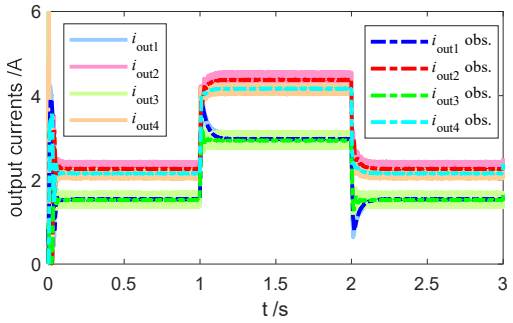

Fig. 5 Real and observed output currents of Converters

Fig. 5 shows the real and observed output currents of each converter. It can be seen that the observed output currents have almost no ripples and can converge to the average value of the actual output currents quickly, verifying that the observer can effectively estimate the output current and replace the actual output current sensor. However, there is an unavoidable delay between the observed current and the actual current; in addition, the observer has a certain low-pass filtering effect, so the ripple of the observed current is significantly smaller than that of the actual current. To a certain extent, this is equivalent to adding a low-pass filter to the output current, and the filter time constant has an inverse proportional relationship with the observer gain L. In practice, this is equivalent to adding additional virtual inertia to the virtual inertia control[6].

5.2 Comparison Test

Existing VID-Control in [10] is tested as comparison test. The existing method designs virtual inertia and damping parameters according to the converter capacity. The virtual inertia and damping are $J_{1,2,3,4}$ = 0.1,0.133,0.1,0.13, $D_{1,2,3,4}$ = 1.05, 1.4, 1.05, 1.4, droop

coefficients are $k_{d,1/2/3/4}$ = 0.4, 0.3, 0.4, 0.3, low-level voltage control parameters are [-0.4, -0.0237, 14.4], [-1.96, -0.0594, 29.6], [-0.44, -0.0237, 14.4], [-1.96, --0.0594, 29.6]. As shown in Fig. 6, this method can effectively improve the bus voltage inertia: when the load is switched, the bus voltage changes slowly, avoiding the rapid voltage change in droop control. However, it results in heavy voltage ripples. As shown in Fig. 7, the output currents of the converters still have certain oscillations, which also lead to heavy bus voltage ripples. On the other hand, the output current has a large oscillation range; when the system load is high, this may trigger the overcurrent protection of the converter and cause it to go off-grid, and even lead to cascading overcurrent protection and off-grid of multiple converters, resulting in system voltage collapse.

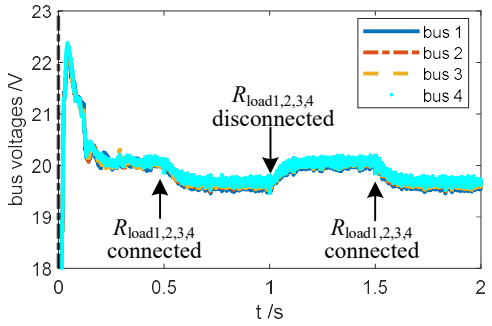

Fig. 6 Bus voltages of existing VID-Control in [10]

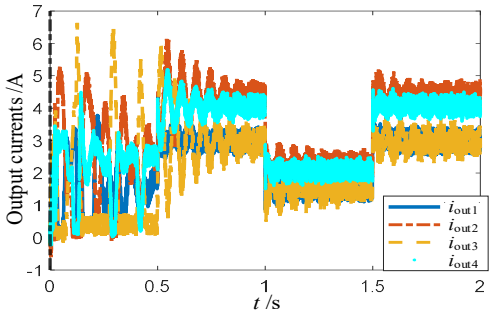

Fig. 7 Output Currents of existing VID-Control

6. CONCLUSION

Based on Lyapunov stability theory, this paper designs an observer-based virtual inertia damping control for multi-bus DC microgrids. By minimizing the coupling between subsystems in the system Lyapunov stability matrix, the decentralized design of virtual inertia and bottom-layer voltage control for each converter is realized, which does not require global system parameters. Experimental results show that the proposed method effectively improves the damping and inertia of the DC microgrid, alleviates the impact of load switching on the bus voltage, suppresses current oscillations between converters, and enhances system stability.

REFERENCE

[1] X. Li, C. Hu, Observer-based Distributed Self-triggered Secondary Control of Multi-bus DC Microgrid Over Directed Communication[J], Proceedings of the China Society Electrical Engineering, 2024,44(22):8771-8786 (in Chinese).

[2] G. Yang, L. Ding, "Distributed Accurate Current Sharing for Multi-Bus DC Microgrids With Minimizing Voltage Regulation Deviations: A Game-Theoretic Approach," in IEEE Transactions on Smart Grid, vol. 16, no. 4, pp. 2725-2737, July 2025.

[3] X. Li, C. Hu, "Distributed Hybrid-Triggered Observer-Based Secondary Control of Multi-Bus DC Microgrids Over Directed Networks," in IEEE Transactions on Circuits and Systems I: Regular Papers, vol. 72, no. 5, pp. 2467-2480, May 2025.

[4] M. Haddadi, S. A. Gorji, "An Overview of Inertia Emulation Strategies for DC Microgrids: Stability Analysis and AC Microgrid Analogies," in IEEE Open Journal of the Industrial Electronics Society, vol. 6, pp. 491-521, 2025.

[5] G. Lin, W. Zuo, "Comparative analysis on the stability mechanism of droop control and VID control in DC microgrid," in Chinese Journal of Electrical Engineering, vol. 7, no. 1, pp. 37-46, March 2021.

[6] ZENG Guohui, LIAO Hongfei. A self-adaptive control strategy of virtual inertia and a damping coefficient for bidirectionalDC-DC converters in a DC microgrid[J].Power System Protection and Control,2022,50(6):65-73 (in Chinese).

[7] G. Lin et al., "A Virtual Inertia and Damping Control to Suppress Voltage Oscillation in Islanded DC Microgrid," in IEEE Transactions on Energy Conversion, vol. 36, no. 3, pp. 1711-1721, Sept. 2021.

[8] ZHANG Kexin, ZHU Lin, et al. Virtual Inertia Evaluation and Coordinated Design of Control Parameters for Multi-converter DC System[J]. Automation of Electric Power Systems, 2024, 48(10):87-95 (in Chinese).

[9] G. Lin, Y. Li, Y. Han, "Dynamic Interaction Stabilization Method for Multi-parallel Hybrid Energy Storage Supplied Electric Vehicle DC Charging Station," in IEEE Transactions on Transportation Electrification, vol. 10, no. 4, pp. 9304-9315, Dec. 2024.

[10] Xialin Li et al., "Observer-Based DC Voltage Droop and Current Feed-Forward Control of a DC Microgrid," in IEEE Transactions on Smart Grid, vol. 9, no. 5, pp. 5207-5216, Sept. 2018.